Vibrational dynamics of 1,3-propanediol in liquid, polycrystalline and glassy states: a Raman spectroscopic study

Vlasta Mohaček-Grošev [a,1*] and Nikola Baran [a]

[a] Centre for Advanced Materials and Sensing Devices, Division of Materials Physics, Ruđer Bošković Institute, Bijenička cesta 54, 10002 Zagreb, Croatia

Abstract

Vibrational transitions of 1,3-propanediol in liquid and crystal phases are assigned on the basis of Raman and infrared spectra of liquid and low temperature (295 K – 10K) Raman spectra which are presented here for the first time. In the crystal, there are four molecules per unit cell, each having a gGGg' conformation. The vibrations for the $P2_1/n$ crystal phase having four molecules in the unit cell are obtained by an ab initio calculation using CRYSTAL09 program, and are in good agreement with the observed Raman bands. Observed bands in Raman spectrum of liquid are in proximity of those observed for crystal phase, and it is tempting to assign them as belonging mainly to gGGg' conformer. However, quantum chemical ab initio calculations provide basis to ascertain that tGG'g and tGGt are two conformers having lowest energy at the B3LYP/6-31++G(d,p) level of theory. Several bands that disappear from Raman spectrum of liquid on solidification (384, 872 and 1040 cm^{-1}) could give an insight into the nature of conformers present in liquid. Since the closest calculated vibrations are 386 cm^{-1} for tGG'g and 1043 cm^{-1} for tGG't conformer, we conclude that all three conformers: tGG'g, tGGt and gGGg', are present in the liquid.

keywords: low temperature Raman spectroscopy, normal modes, CRYSTAL09, phonons, conformational analysis, renewable polymers

prepared for Spectrochimica Acta A: Molecular and Biomolecular Spectroscopy

doi: 10.1016/j.saa.2019.117567

[1] corresponding author, e-mail:mohacek@irb.hr

1 Introduction

The rise of awareness concerning the amount of insoluble plastic ending in environment as well as limited amount of petroleum-based materials has stimulated research and production both of biodegradable and renewable polymers [1]. Until the last few years, less attention was paid to plastic products after their lifetime. This has changed, however, as new legislation procedures are being implemented in European Union and worldwide [2,3]. The market for 1,3-propanediol (PDO) amounts currently to over 100 million pounds per year and is growing rapidly [4]. The reason for this is that PDO can replace ethylene glycol and butylene glycol in the synthesis of polyesters and polyurethanes, in particular for polymethylene terephtalate [4,5]. In order to minimize greenhouse emission and consume less energy, the procedure for obtaining PDO has turned to microbial production based either on glycerol or on glucose [4,6,7]. Also, a research proposing PDO as a potential substitute of propylene glycol in refill liquid for electronic cigarettes has recently been published [8]. Vibrational spectroscopy is a well established experimental tool for process monitoring [9,10], often used in chemical plants and pharmaceutical companies [11]. It is therefore of interest to present vibrational spectroscopic characteristion of 1,3-propanediol.

Conformational states of 1,3-propanediol have been studied by Johansson in 1973 [12] and more thoroughly by Bultinck et al in 1995 [13]. Using *ab initio* methods Bultinck et al. optimized geometries of twenty three conformers and found that the most stable conformer had gauche O-C-C-C torsional angle. Semiempirical study of Friedemann and Jabs included monomers, dimers and monohydrates of PDO [14]. They found that intramolecular hydrogen bonds were preserved in dimers. Kinneging et al. performed an electron diffraction study on PDO which confirmed the existence of an intramolecular hydrogen bond [15]. The energy of the intramolecular hydrogen bond in 1,3-propandiol was estimated using quantum theory of atoms in molecules (QTAIM) by Mandado and coworkers in 2006 [16]. Takahashi studied the effect of hydrogen bonding on OH stretching overtone decay lifetime [17], while Muniz-Miranda et al. undertook Car-Parrinello molecular dynamics simulation of PDO/acetonitrile solutions and compared calculated vibrational density of states with the experimental infrared spectra in order to elucidate spectral components of intra- and intermolecular hydrogen bonding [18]. Thalladi, Boese and Weiss examined melting point alternation in alkanediols and reported the crystal structure of 1,3-propanediol to be $P2_1/n$ with Z=4 molecules per unit cell, a = 4.9396 Å, b = 7.9436 Å, c = 10.6007 Å, β = 90.097° [19]. Emel'yanenko and Verevkin authored benchmark thermodynamic study of 1,3-propanediol which used vapour pressure temperature dependence measurements for the derivation of molar enthalpy of vaporisation [20]. They also calculated thermal populations of each PDO conformer using G3MP2 under Gaussian09, and predicted that 40 % of free PDO molecules have tGG'g conformation, 20 % gGG'g conformation, and 18 % tGG't conformation (in Bultinck notation).

Vibrational studies of 1,3-propanediol are scarce. Both Busfield et al. [21] and Shagidullin with coworkers [22] performed an infrared study of dilute solutions of PDO in carbon tetrachloride in order to study intramolecular hydrogen bonding. Shagidullin et al. presented also infrared spectra of the PDO in gas phase and discussed temperature dependence of some Raman bands, but did not give a complete list of

bands with proper assignment [22]. Both groups concentrated on the O-H stretching spectral region.

In this work Raman and infrared specta of liquid are reported and the observed bands interpreted on the basis of normal mode calculation for a set of five conformers. Several Raman bands disappearing on solidification are singled out and discussed. Also, temperature dependent Raman spectra starting form 295 K to 10 K are presented for the first time. In the crystal, 1,3-propanediol molecules take up the gGGg' conformation. Low temperature Raman phonons observed for polycrystalline PDO are assigned on the basis of an *ab initio* optimization of the crystal structure and frequencies calculation done by CRYSTAL09 program. Furthermore a glassy state was observed on freezing of the liquid to 160 K and lower temperatures.

2 Experimental

1,3-Propanediol was purchased from Aldrich as 98 % pure liquid. On opening the bottle, approx. 100 µl of the liquid was transferred by a syringe into a capillary connected to vacuum line. Using a freeze-pump-thaw procedure, repeated degassing of N_2 and O_2 from the sample was done. Once sealed, the capillary was mounted onto the cold finger of a closed cycle helium optical cryostat CCS 350 from Janis Research, connected to the Lake Shore 331 temperature controller.

Raman spectra were recorded with T64000 Horiba-JobinYvon spectrometer in the triple subtractive configuration, using both single window and multiwindow options. For excitation, a semiconductor laser DPSS 532 nm from Changchun New industries Optoelectronics Tech. was used. Liquid nitrogen cooled CCD detector for VIS region with 1024 x 256 pixels served as a detector. Spectral resolution was 0.6 cm^{-1} per pixel. Average acquisition time was 20 seconds and four scans were averaged for the final result.

Infrared spectrum was recorded using a Perkin Elmer liquid cell with two circular KBr windows with a 20 µm spacer between. The empty cell was used for background recording with a SPECTRUM GX Perkin Elmer Fourier transform spectrometer. For sample spectrum recording 1 µl drop of propanediol was put on one window, covered with spacer and the other window and tightly pressed with screws. Fifty scans with 4 cm^{-1} resolution were chosen set of conditions.

3 Computational details

Normal mode calculations for tGG'g, tGGt, gGGg', gGG'g and tTTt conformers were performed with the Gaussian09 program [23]. The geometry of the propanediol was optimized using B3LYP functional with 6-31++G(d,p) basis set, without imposing symmetry restrictions upon geometry. For potential energy distribution calculation BALGA program was used [24,25]. Definition of internal coordinates is given in Supplementary table S1, while local symmetry coordinates are listed in Supplementary table S2. Finally, a detailed potential energy distribution for tGG'g and tGGt conformers is presented in Table 1, while for tTTt conformer it is given in Supplementary table S3 and for gGGg' in the Supplementary table S4.

For the *P21/n* crystal structure partial optimization of atomic positions with fixed cell parameters was performed first using density functional theory as implemented in CRYSTAL09 program [26]. The correlation functional of Lee, Yang and Parr [27] with generalized gradient approximation and the exchange functional of Becke [28] popularly kown as B3LYP functional were used.
When the SHRINK keyword defining the grid of k points was set to 4, 4 and 2, the total energy of the crystal was ET = -1077,7779 Hartree without dispersion correction and –1077,9252 Hartree when dispersion correction as described by Grimme [29] was taken into account. The convergence criteria for energy during geometry optimization was set to 10^{-7} Hartree, whereas for calculation of vibrations it was 10^{-10} Hartree. Extra large grid was used. Basis sets for carbon, hydrogen and oxygen of the 6-31G** type were transferred from the study of urea by Gatti et al [30]. This basis set has been found adequate for calculations on molecular crystals by Barone [31]. The calculations were run on HP Z640 workstation using eight processors.

4 Results and Discussion

4.1 Conformational analysis of liquid propanediol

Previous conformational studies of PDO were conducted by Bultinck et al. [13] and Emel'yanenko and Verevkin [20], while Mandado et al. [16] inspected just three conformers displaying intramolecular hydrogen bonding. The capital letters G and G' refer to positive or negative torsional angle of *gauche* conformation with respect to the torsion around one or the other C-C bond. Small t or g letters refer to *trans* or *gauche* conformation for the rotation around C-O bonds. Both Bultinck et al. and Emel'yanenko and Verevkin found there are three conformers within the 2 kJ/mole energy difference, and both groups concluded that the tGG'g is the most stable conformation of PDO. The second conformer in the order of rising energies is found by both groups to be gGG'g, but in the third conformer the predictions of two groups differ. Bultinck et al. calculated the tGGg' conformation to be 6.96 kJ/mol above the energy of the tGG'g, while Emel'yanenko and Verevkin reported that the third conformation in the rising order is tGG't and has only 2.03 kJ/mol higher energy than the tGG'g. We repeated the calculations for tGG'g and gGG'g coformers, and included also gGGg' conformation that is found in crystal state as well as tGGt and tTTt. Using B3LYP/6-31++G(d,p) level of theory, we found that tGG'g is the most stable conformer, followed by tGGt (6.82 kJ/mol higher energy), gGGg' (8.36 kJ/mol higher), gGG'g (10.77 kJ/mol higher) and tTTt (13.39 kJ/mol higher than the energy of tGG'g). In the units of Hartree, the energies of the three most stable conformations are -269.5949925 Ha (tGG'g), -269.5923931 Ha (tGGt),and -269.591806414 Ha (gGGg') (see Fig 1). Since we obtained all positive frequencies of normal modes for all five conformers, we find them stable. On the contrary, Mandado et al. [16] stated that tGG'g conformer was not a stable one (they used B3LYP/6-311++G(2d,2p) procedure).

For the three conformers having lowest energy one can compare thirty three positive frequencies with the observed Raman and infrared bands for liquid and crystalline

PDO (Figs 2 and 3, Supplementary figs S2 – S5, Tables 1 and 2, Supplementary table S4). The tGGg' and gGGg' conformers have no symmetry elements, and the tGGt has one C_2 axes. Hence, in each case all thirty three modes are observable both in Raman and infrared spectra of liquid. In Table 1 the calculated unscaled vibrations belonging to the tGG'g conformer (τ_1 = -175.8°, τ_2 = 59.6°, τ_3 = -72.4°, τ_4 = 46.8°) and tGGt (τ_1 = -172.2°, τ_2 = 65.4°, τ_3 = 65.4°, τ_4 = -172.4°) are compared with Raman and infrared bands of liquid and Raman bands observed for polycrystalline PDO. Calculated normal modes of the gGGg' conformer are given in Supplementary table S4. Its torsional angles obtained upon geometry optimization are τ_1 = 66.9°, τ_2 = 50.9°, τ_3 = 54.9°, τ_4 = -78.8°.

Many observed bands in Raman spectra of liquid and crystal have very close wavenumbers, and it is tempting to assign them belonging mainly to gGGg' conformer. From skeletal deformation modes which are usually observed below 600 cm^{-1} one can make an attempt to deduce which conformer is present in liquid. In the infrared spectrum of liquid a band at 528 cm^{-1} is found, whereas in Raman spectrum of liquid one observes bands at 529, 412, 384 and 278 cm^{-1}. The band at 384 cm^{-1} observed in Raman spectrum of liquid disappears on freezing (Fig 3), just as the bands observed at 872 cm^{-1} and 1040 cm^{-1}. The 412 cm^{-1} and 529 cm^{-1} Raman bands observed in liquid have their counterparts in 445 cm^{-1} and 535 cm^{-1} bands in Raman spectrum of solid at 170 K (Fig 3).

Before discussing the origin of the forementioned bands, let us remind ourselves of the lowest frequency modes of propane. The C-C-C bending band was attributed to the 369 cm^{-1} band, and the methyl torsions to 208 and 223 cm^{-1} bands [32]. Between 400 and 740 cm^{-1} no fundamental was assigned, but a methylene rocking band was observed at 748 cm^{-1}. In 1,3-propanediol seven low frequency modes below 700 cm^{-1} are expected: a C-C-C bending, two -CH_2OH torsional vibrations, two -OH torsional and two C-C-O bending vibrations. The actual values of normal modes frequencies that are calculated correspond to the gas phase, whereas the positions of measured bands given in Table 1 refer to condensed phases. Therefore, large discrepancies between calculated and observed wavenumbers are expected for modes involving -OH groups. The C-C-C skeletal bending mode is predicted at 330 cm^{-1} for tGG'g conformer, at 239 cm^{-1} (mixed) for gGGg' conformer and at 528 cm^{-1} for tGGt conformer. Two O-C-C bending modes are calculated to be 386 and 192 cm^{-1} for tGG'g conformer, at 415 and 265 cm^{-1} for tGGt conformer, and at 572 and 405 for gGGg' conformer.

On freezing, one observes at 10 K Raman bands at 535, 445, 306, 300, and 278 cm^{-1}, the bands at 306 and 300 being interpreted as crystal splitting of the one internal mode. The disappearance of the 384 cm^{-1} Raman band from liquid is interesting in view of the existing conformation of PDO molecules in crystal: they all have gGGg' conformation: τ_1 = 67.6°, τ_2 = 61.5°, τ_3 = 69.4°, τ_4 = -82.6° (Fig 4). Therefore the 384 cm^{-1} band is attributed to another conformer in liquid, possibly tGG'g. The other two strong bands in Raman spectrum of liquid which disappear on freezing are at 1040 and 872 cm^{-1}. Judging on the basis of calculated values for tGGt conformer that are in proximity - 853 and 1043 cm^{-1} - as well as the bands calculated for tGG'g conformer at 905 and 1076 cm^{-1}, one could assign the 1040 cm^{-1} band to the tGGt conformer (see Fig 5 for comparison of calculated and observed spectral intensities for different

conformers). In Supporting Material all Gaussian09 output files for the tGG'g, tGGt and gGGg' are given, including the tTTt conformer. The tTTt conformer was included because of the possibility that end-to-end hydrogen bonding in liquid might prefer *all trans* conformation of PDO molecule, but some bands could not be assigned (printed in italic in the Supplementary table S3).

4.2 Raman spectra of polycrystalline propanediol

Propanediol is a transparent, slightly oily liquid, which exhibits significant supercooling and solidifies in polycrystalline form at 170 K when slowly cooled (the melting point reported is 246 K [34]). On rapid cooling, it forms a glassy state, whose Raman spectrum is at the top in Fig 2. The lowest band observed in glassy state at 10 K is found at 51 cm^{-1} (Supplementary Fig S5), whereas the Bose peak characteristic for disordered systems was measured in 1,3-propanediol liquid at 24 cm^{-1} [35]. The 51 cm^{-1} band was attributed to the torsional modes of methoxy groups. The space group of the PDO crystal is $P2_1/n$ with four molecules per unit cell [19], see Fig 4. No atom is situated on any of the symmetry elements in the cell and the expected number of vibrations (phonons) is:

$$\Gamma_{TOT} = 39\,A_g \oplus 39\,B_g \oplus 38\,A_u \oplus 37B_u.$$

Phonons of the A_g and B_g symmetry are Raman active, while those of A_u and B_u symmetry are infrared active. Below 250 cm^{-1} one expects collective librational and translational modes of the symmetry:

$$\Gamma_{ext} = 6\,A_g \oplus 6\,B_g \oplus 5\,A_u \oplus 4\,B_u.$$

Within rigid molecule approximation, librations are Raman active, since their symmetry is of the *gerade* type, while translational modes are infrared active because they belong to A_u and B_u irreducible representations. Therefore in low frequency Raman spectrum one expects at least 12 modes, but seven are observed (Supplementary Fig S5, Table 2). The majority of bands occur at slightly shifted wavenumbers with respect to those observed in liquid, the exception being of course bands corresponding to modes involved in hydrogen bonding. For every internal mode that is observable in liquid spectrum, there are four corresponding phonons in the crystal, of A_g, B_g, A_u and B_u symmetry. Therefore for every band observed in Raman spectrum of liquid, one expects two new bands in the Raman spectrum of crystal. Sometimes not all vibrational modes could be resolved in liquid, such as in the case of C-H stretching bands which we expect six, but observe three: at 2887, 2913 and 2958 cm^{-1}. At 10 K one observes seven out of eight expected bands: 2881, 2889, 2908, 2917, 2943, 2954 and 2978 cm^{-1}. In Supporting Material the list of calculated phonons by CRYSTAL09 program is presented. In Table 2. a partial list of calculated phonons below 550 cm^{-1} is given, where good agreement between observed and calculated bands positions is found.

4.3 Vibrations involving hydrogen bonded atomic groups

There are two types of intermolecular O-H···O hydrogen bonds in the PDO crystal, corresponding to O···O distances of 2.698 Å and 2.722 Å (see Fig 4). According to Novak [34] these would be weak hydrogen bonds with **ν**(OH) above 3200 cm^{-1}. Indeed, one finds three out of four expected broad bands at 10 K: at 3265, 3250 and 3159 cm^{-1}. The δ(C-O-H) bending modes are mixed with other modes, in particular with δ(H-C-C) and δ(H-C-O) angle deformation vibrations, and significantly contribute to 1191 and 1222 cm^{-1} modes attributed to the tGG'g conformer (Table 1). The potential energy distribution shows that 1052 cm^{-1} mode of the gGG'g conformer has a significant contribution of the δ(C-O-H) bending vibration (Supplementary material). The torsion of hydroxyl groups is assigned to a very broad band in the infrared spectrum observed at 666 cm^{-1} (Supplementary figure S2), and it could correspond to a weak 695 cm^{-1} band observed in Raman spectrum of polycrystalline sample at 10 K (Fig 3).

4 Conclusion

The assignment of normal modes of 1,3-propanediol has been given on the basis of Raman and infrared bands observed in spectra of liquid. Good agreement has been achieved in assigning the majority of observed bands as belonging to tGG'g and tGGt conformers. The band observed at 384 in Raman spectrum of liquid is assigned to the OCC bending of the tGG'g conformer. It disappears from Raman spectrum on solidification, just as the bands at 872 and 1040 cm^{-1} . The 1040 cm^{-1} band could be assigned to the tGGt conformer since a 1043 mode is predicted for its C-C bending motion. Raman spectra of solid 1,3-propanediol were recorded from 295 K to 10 K. No indications of a phase transition have been found – the number of external phonons remains the same throughout the temperature interval studied (170 K – 10 K). When rapidly cooled, propanediol solidifies in a glassy state.

Acknowledgement

This work was partially supported by Centre of Excellence for Advanced Materials and Sensors, a project co-financed by the Croatian government and the European Union through the European regional development fund – The Competitivness and Cohesion Operational Programme (KK.01.1.1.01). Calculations using Gaussian09 were performed at University of Zagreb Computing Centre SRCE.

References

1. http://www.weforum.org/agenda/2018/08/the-world-of-plastics-in-numbers/

2. https://www.plasticseurope.org/application/files/5715/1717/4180/Plastics_the_facts_2017_FINAL_for_website_one_page.pdf

3. „A European Strategy for Plastics in a Circular Economy“, Commission Staff Working Document, http://ec.europe.eu/environment/circular-economy/index-en.htm.

4. H. Liu, Y. Xu, Z. Zheng, D. Liu, Biotechnology J. 5 (2010) 1137 – 1148.

5. T. Debuissy, P. Sangwan, E. Pollet, L. Avérous, Polymer 122 (2017) 105 -116.

6. X. Yang, D. S. Kim, H. S. Choi, C. K. Kim, L. P. Thapa, C. Park, S. W. Kim, Chem. Eng. J. 314 (2017) 660 -669.

7. E. Tabah, A. Varvak, I. Neel Pulidindi, E. Foran, E. Banin, A. Gedanken, Green Chemistry 18 (2016) 4657.

8. P. Bertrand, B. Bonnarme, A. Piccirilli, P. Ayrault, L. Lemée, G. Frapper, J. Pourchez, Scientific Reports 8 (2018) 10702.

9. T. DeBeer, A. Burggraeve, M. Fonteyne, J. P. Remon, C. Vervaet, Int. J. Pharmaceutics 417(1-2) (2011) 32-47.

10. http://www.recendt.at/en/IR.html

11. K. Buckley, A. G. Ryder, Applied Spectroscopy 71(6) (2017) 1085 – 1116.

12. A. Johansson, P. Kollman, S. Rothenberg, Chem. Phys. Lett. 18 (1973) 276 – 279.

13. P. Bultinck, A. Goemine, D. Van de Vondel, J. Mol. Struct. (Theochem) 357 (1995) 19 – 32.

14. R. Friedemann, A. Jabs, J. Mol. Struct. (Theochem) 283 (1993) 191 – 197.

15. A. J. Kinneging, V. Mom, F. C. Mijlhoff, G. H. Renes, 82 (1982) 271 – 275.

16. M. Mandado, R. A. Mosquera, C. Van Alsenoy, Tetrahedron 62 (2006) 4243 – 4252.

17. K. Takahashi, Physical Chemistry Chemical Physics 12 (2010) 13950 -13961.

18. F. Muniz-Miranda, M. Pagliai, G. Cardini, R. Righini, J. Chem. Phys. 137 (2012) 244501.

19. V. R. Thalladi, R. Boese, H.-C. Weiss, Angew. Chem. Int. Ed. 39 (2000) 918 – 922.

20. V. N. Emel'yanenko, S. P. Verevkin, J. Chem. Thermodynamics 85 (2015) 111 – 119.

21. W. K. Busfield, M. P. Ennis, I. J. McEwen, Spectrochim. Acta A 29 (1973) 1259 – 1264.

22. Rif. R. Shagidulin, A. V. Chernova, A. Kh. Plyamovtyi, R. R. Shagidullin, Bull. Acad. Sci. USSR 40 (10) (1991) 1993 – 1999.

23. Gaussian 09, Revision A.02, M. J. Frisch, G. W. Trucks, H. B. Schlegel, G. E. Scuseria, M. A. Robb, J. R. Cheeseman, G. Scalmani, V. Barone, G. A. Petersson, H. Nakatsuji, X. Li, M. Caricato, A. Marenich, J. Bloino, B. G. Janesko, R. Gomperts, B. Mennucci, H. P. Hratchian, J. V. Ortiz, A. F. Izmaylov, J. L. Sonnenberg, D. Williams-Young, F. Ding, F. Lipparini, F. Egidi, J. Goings, B. Peng, A. Petrone, T. Henderson, D. Ranasinghe, V. G. Zakrzewski, J. Gao, N. Rega, G. Zheng, W. Liang, M. Hada, M. Ehara, K. Toyota, R. Fukuda, J. Hasegawa, M. Ishida, T. Nakajima, Y. Honda, O. Kitao, H. Nakai, T. Vreven, K. Throssell, J. A. Montgomery, Jr., J. E. Peralta, F. Ogliaro, M. Bearpark, J. J. Heyd, E. Brothers, K. N. Kudin, V. N. Staroverov, T. Keith, R. Kobayashi, J. Normand, K. Raghavachari, A. Rendell, J. C. Burant, S. S. Iyengar, J. Tomasi, M. Cossi, J. M. Millam, M. Klene, C. Adamo, R. Cammi, J. W. Ochterski, R. L. Martin, K.

Morokuma, O. Farkas, J. B. Foresman, and D. J. Fox, Gaussian, Inc., Wallingford CT, 2016.

24. G. Keresztury, G. Jalsovszky, J. Mol. Struct. 10 (1971) 304–305.

25. H. Rostkowski, L. Lapinski, M. Nowak, Vib. Spectrosc. 49 (2009) 43–51.

26. R. Dovesi, R. Orlando, B. Civalleri, C. Roetti,V. R. Saunders, C. M. Zicovich-Wilson, CRYSTAL: a Computational Tool for the Ab Initio Study of the Electronic Properties of Crystals Z. Kristallogr. 220 (2005) 571-573.

27. C. Lee, W. Yang, R. G. Parr, Phys. Rev. B 37 (1988) 785-789.

28. A. D. Becke, Phys. Rev. A 38 (1988) 3098-3100.

29. S. Grimme, J. Comput. Chem. 27 (2006) 1787-1799.

30. C. Gatti, V. R. Saunders, C. Roetti, J. Chem. Phys. 101 (1994) 10686-10696.

31. V. Barone, J. Chem. Phys. 122 (2005) 014108.

32. J. N. Gayles Jr., W. T. King, J. H. Schachtschneider, Spectrochim. Acta A 23 (1967) 703 – 715.

33. https://web.archive.org/web/20041227154049/http://www.shellchemicals.com/chemicals/pdf/pdo/brochure.pdf?section=our_products

34. A. Novak, „Structure and Bonding“, vol. 18, Springer Verlag 1974. p. 177 – 216.

35. O. Yamamura, K. Harabe, T. Matsuo, K. Takeda, I. Tsukushi, T. Kanaya, J. Phys.: Condens. Matter 12 (2000) 5143–5154.

Table 1. Unscaled normal modes of tGG'g and tGGt 1,3-propanediol are compared with the observed bands. Potential energy distribution (PED) among symmetrized coordinates is calculated by BALGA[†] program. Contributions greater than 10% are given. v-very, s-strong, m-medium, w-weak, sh-shoulder, br-broad

observed Raman liquid	observed Raman cryst 10 K	observed infrared liquid	calculated		calculated	
			tGG'g	PED (%) tGG'g	tGGt	PED (%) tGGt
3309 w, vbr		3335 vs, vbr				
	3250 m		3841	83 S_1	3842	100 S_1
	3236 mw		3761	86 S_{18}	3842	100 S_{18}
	3135 m, br					
	2978 ms					
2958 s, sh	2954 s,sh		3087	72 S_{28} + 15 S_{19}	3090	92 S_{28}
	2943 vs	2945 s	3084	25 S_{19} + 22 S_{12} + 20 S_{28}	3062	75 S_{12} + 18 S_3
	2927 s		3044	35 S_{12} + 35 S_3	3055	82 S_{19} + 11 S_{27}
2913 vs	2908 vs	2883 s	3032	58 S_3 + 23 S_{19} + 18 S_{12}	3042	79 S_3 + 11 S_2 + 11 S_{11}
2887 vs	2889 m, sh		2999	50 S_2 + 46 S_{27}	3005	80 S_2 + 15 S_{12}
	2881 s		2967	33 S_{27} + 29 S_2 +20 S_{12}	3004	86 S_{27} + 13 S_{19}
					1523	72 S_{24} + 24 S_{23}
1476 ms	1477 s	1474 ms	1524	58 S_{24} + 12 S_4	1520	66 S_9 + 28 S_8
	1463 m		1510	78 S_9 + 14 S_{24}		
1440 m	1450 m		1468	59 S_{23} + 20 S_{24} + 15 S_{11}	1466	87 S_{10}
					1448	53 S_8 +25 S_9 + 11 S_{11}
1426 m, sh		1433 s	1446	86 S_{10}	1433	38 S_{23} +14 S_{25} +14 S_{26}
	1413 s		1443	52 S_8 + 22 S_{26} + 17 S_9		
	1391 w		1388	22 S_{31} + 17 S_{24} + 10 S_{11}	1390	54 S_{25} + 22 S_{23}
	1366 w	1377 ms	1373	24 S_8 + 23 S_{25} + 22 S_{11}		
1316 m,sh	1348 w	1355 ms	1302	40 S_{15} + 22 S_{14} + 11 S_{24}	1326	51 S_{14} + 23 S_{13}
1294 ms	1294 s	1292 m	1273	72 S_{29} + 13 S_{13}	1274	46 S_{15} + 23 S_{11} +16S_{13}
1238 m	1228 mw	1231 m	1222	43 S_{26} + 39 S_{15} + 16 S_{13}	1265	31 S_{26} +30 S_{31} + 16 S_{29}
1193 m	1189 s	1184 m	1191	35 S_{11} + 24 S_{14} + 19 S_{23}	1239	49 S_{31} + 28 S_{26}

1097 m, sh	1086 m	1063 vs	1132	54 S_{31} + 16 S_{30}	1168	50 S_{11} + 19 S_{15} + 16 S_{14}
1062 ms	1062 m	1038 s	1088	42 S_4 + 14 S_{20} + 11 S_{21}	1123	27 S_{13} + 21 S_4 +20 S_{15}
1040 m, sh		986 s	1076	47 S_{21} + 13 S_{25}	1092	54 S_{20} + 17 S_{21} + 12 S_{30}
986 m	992 s	940 m				
941 m	947 m	921 m			1043	42 S_{21} + 27 S_{26} + 15 S_{30}
920 m	935 m	869 w	954	47 S_{13} + 19 S_{15}	998	67 S_4 + 15 S_{13} +12 S_{14}
872 s		847 w	912	32 S_{20} +25 S_{30}	965	35 S_{20}+ 34 S_{29} +13 S_{25}
850 s	853 vs		905	69 S_5 + 10 S_{30}		
815 w	808 w	782 m			853	78 S_5
782 w	774 m		814	36 S_{20} +23 S_7+15 S_4+15 S_{31}	793	42 S_{30} + 26 S_{29} + 13 S_{20}
	714 w	666 m, vbr	192	71 S_{32} + 13 S_6	167	80 S_{32} + 15 S_{33}
		528 m				
529 mw	535 m					
412 w	445 w		531	48 S_{17} + 18 S_{33}	529	47 S_7 + 28 S_6
			504	68 S_7 + 22 S_{30}	417	69 S_{22} + 19 S_{30}
384 w						
	306, w 300 sh		386	93 S_{22}		
278 vw	278 w		330	46 S_6 + 15 S_{33} + 13 S_{17}		
	220 mw		280	30 S_{33} + 23 S_{17} + 14 S_6	266	33 S_7 + 32 S_{17} + 31 S_6
	187 vw				239	63 S_{17} + 21 S_6
	124 w				238	83 S_{33} + 13 S_{32}
	102 w			100 S_{16}		
	80 w, sh		106		87	93 S_{16}
	75 m					
	47 w					

Table 2. Low frequency Raman bands of polycrystalline PDO observed at 10 K compared to values calculated by CRYSTAL09 program. For complete list of all phonons see Supplementary Material.v-very, s-strong, m-medium, w-weak, sh-shoulder, br-broad

Partial list of calculated Raman phonons (cm^{-1})		observed Raman bands below 550 cm^{-1} at 10K (cm^{-1})
symmetry	value	value
B_g	545	
A_g	541	535
A_g	466	445
B_g	453	
B_g	322	306
A_g	322	300 sh
B_g	290	
A_g	287	278
A_g	242	220
A_g	205	187
B_g	191	
A_g	155	
B_g	145	
A_g	135	124
B_g	126	
B_g	109	
A_g	108	102
A_g	88	80
A_g	73	75
B_g	73	
B_g	64	
A_g	55	47

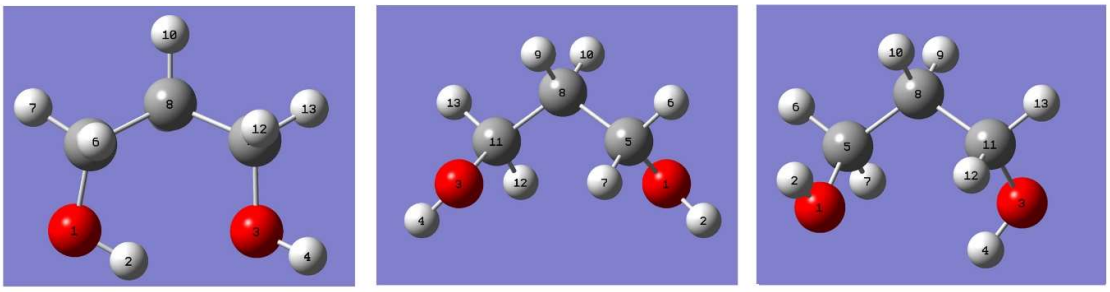

Figure 1. Labelling of atoms in 1,3-propanediol. Three most stable conformers are tGG'g , tGGt, and gGGg' (this work).

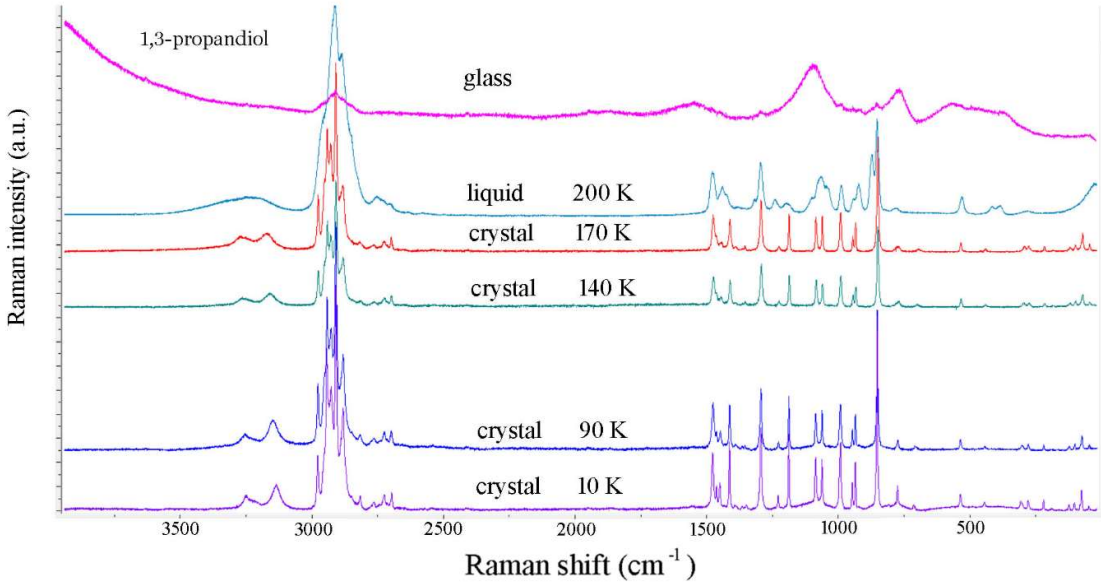

Figure 2. Comparison of Raman spectra of liquid (200 K) with Raman spectra of polycrystalline solid (170 K, 140 K, 90 K and 10 K) and glass (10 K).

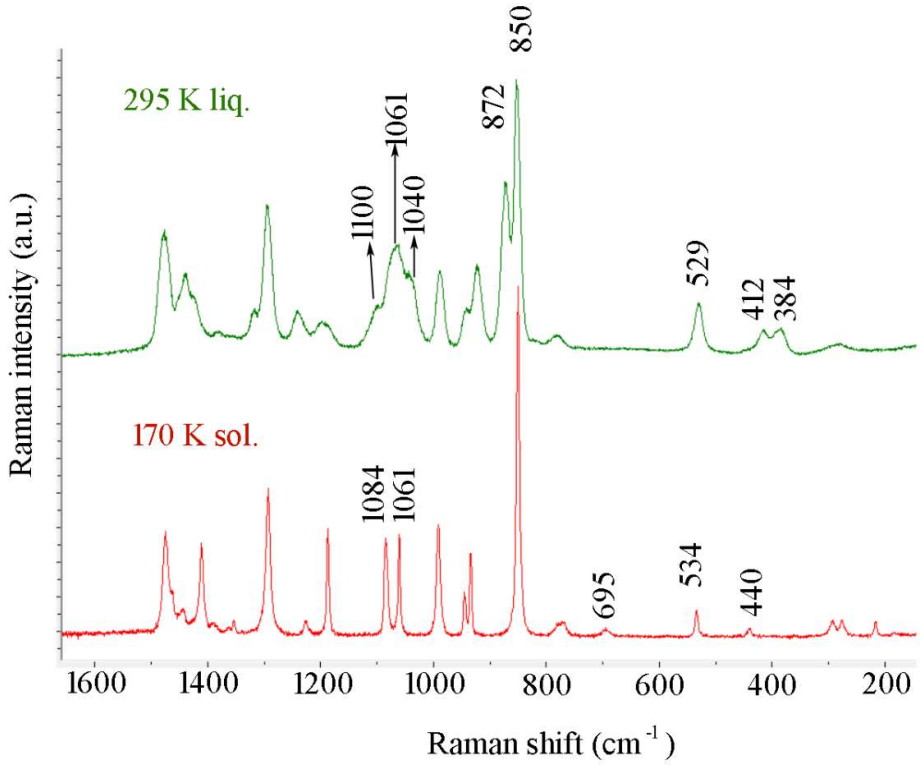

Figure 3. The disappearance of the 384, 872 and 1040 cm^{-1} bands on crystallization of 1,3-propanediol.

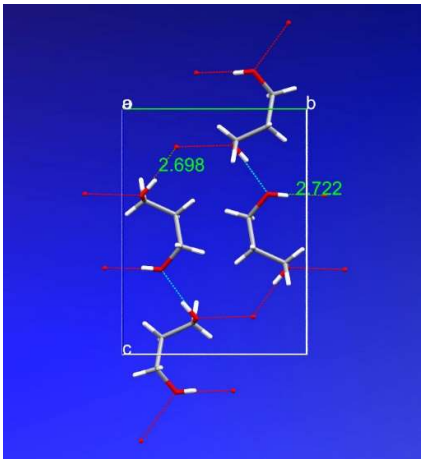

Figure 4. Crystal structure of 1,3-propanediol with two different O…O hydrogen bonds lengths in Å indicated.

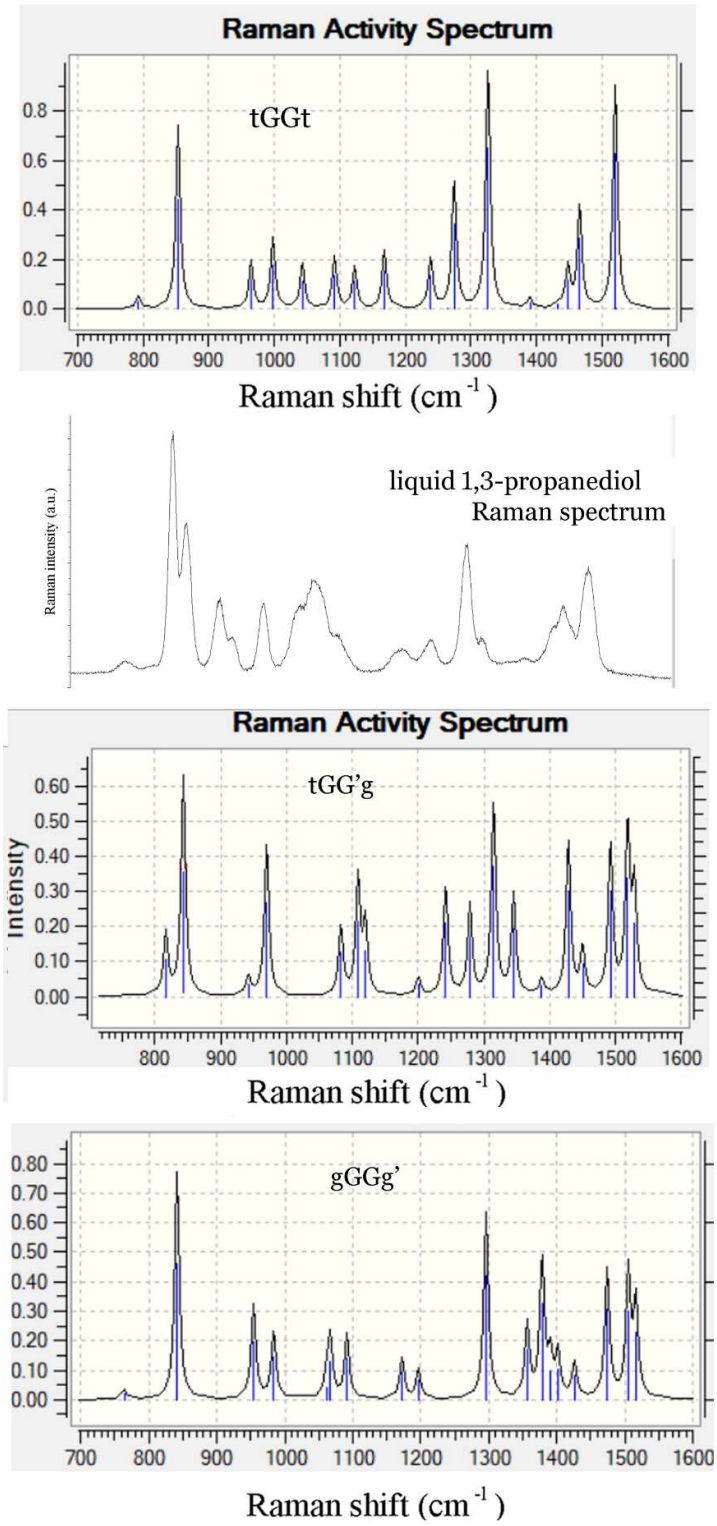

Figure 5. Calculated Raman spectra for three conformers of PDO are compared with the experimental spectrum (700 – 1600 cm^{-1}).

Supplementary table S1. Definition of internal coordinates in 1,3-propanediol.

Deformations of bond stretching coordinates

1. $\Delta l_1 = \Delta(O_1 - H_2)$
2. $\Delta l_2 = \Delta(O_2 - H_4)$
3. $\Delta r_2 = \Delta(C_5 - H_6)$
4. $\Delta r_3 = \Delta(C_5 - H_7)$
5. $\Delta r_5 = \Delta(C_{11} - H_{13})$
6. $\Delta r_6 = \Delta(C_{11} - H_{12})$
7. $\Delta r_7 = \Delta(C_8 - H_9)$
8. $\Delta r_8 = \Delta(C_8 - H_{10})$
9. $\Delta L_1 = \Delta(C_5 - O_1)$
10. $\Delta L_2 = \Delta(C_{11} - O_3)$
11. $\Delta R_1 = \Delta(C_5 - C_8)$
12. $\Delta R_2 = \Delta(C_8 - C_{11})$

Deformations of bond angles coordinates:

13. $\Delta\omega = \Delta(C_5\text{-}C_8\text{-}C_{11})$
14. $\Delta\eta_1 = \Delta(O_1\text{-}C_5\text{-}C_8)$
15. $\Delta\eta_2 = \Delta(O_3\text{-}C_{11}\text{-}C_8)$
16. $\Delta\theta_2 = \Delta(H_6\text{-}C_5\text{-}C_8)$
17. $\Delta\theta_3 = \Delta(H_7\text{-}C_5\text{-}C_8)$
18. $\Delta\theta_5 = \Delta(H_{13}\text{-}C_{11}\text{-}C_8)$
19. $\Delta\theta_6 = \Delta(H_{12}\text{-}C_{11}\text{-}C_8)$
20. $\Delta\alpha_2 = \Delta(H_6\text{-}C_5\text{-}O_1)$
21. $\Delta\alpha_3 = \Delta(H_7\text{-}C_5\text{-}O_1)$
22. $\Delta\alpha_5 = \Delta(H_{13}\text{-}C_{11}\text{-}O_3)$
23. $\Delta\alpha_6 = \Delta(H_{12}\text{-}C_{11}\text{-}O_3)$
24. $\Delta\beta_1 = \Delta(H_9\text{-}C_8\text{-}C_5)$
25. $\Delta\beta_2 = \Delta(H_{10}\text{-}C_8\text{-}C_{11})$
26. $\Delta\beta_3 = \Delta(H_9\text{-}C_8\text{-}C_{11})$
27. $\Delta\beta_4 = \Delta(H_{10}\text{-}C_8\text{-}C_5)$
28. $\Delta\varepsilon_1 = \Delta(H_2\text{-}O_1\text{-}C_5)$
29. $\Delta\varepsilon_2 = \Delta(H_4\text{-}O_3\text{-}C_{11})$

Torsional angle deformations

30. $\Delta\tau_{M1} = \Delta(H_7\text{-}C_5\text{-}C_8\text{-}C_{11}) + \Delta(H_6\text{-}C_5\text{-}C_8\text{-}C_{11}) + \Delta(O_1\text{-}C_5\text{-}C_8\text{-}C_{11})$
31. $\Delta\tau_{M2} = \Delta(H_{13}\text{-}C_{11}\text{-}C_8\text{-}C_5) + \Delta(H_{12}\text{-}C_{11}\text{-}C_8\text{-}C_5) + \Delta(O_3\text{-}C_{11}\text{-}C_8\text{-}C_5)$
32. $\Delta\tau_{OH1} = \Delta(H_2\text{-}O_1\text{-}C_5\text{-}C_8)$
33. $\Delta\tau_{OH2} = \Delta(H_4\text{-}O_3\text{-}C_{11}\text{-}C_8)$

Supplementary table S2. Definition of symmetrized coordinates for tTTt conformer of 1,3-propanediol. The same coordinates are used for other conformers as well.

11 A_1

1. $S_1 = \Delta l_1 + \Delta l_2$
2. $S_2 = \Delta r_2 + \Delta r_3 + \Delta r_5 + \Delta r_6$
3. $S_3 = \Delta r_7 + \Delta r_8$
4. $S_4 = \Delta L_1 + \Delta L_2$
5. $S_5 = \Delta R_1 + \Delta R_2$
6. $S_6 = \Delta\omega$
7. $S_7 = \Delta\eta_1 + \Delta\eta_2$
8. $S_8 = \Delta\theta_2 + \Delta\theta_3 + \Delta\theta_5 + \Delta\theta_6$
9. $S_9 = \Delta\alpha_2 + \Delta\alpha_3 + \Delta\alpha_5 + \Delta\alpha_6$
10. $S_{10} = \Delta\beta_1 + \Delta\beta_2 + \Delta\beta_3 + \Delta\beta_4$
11. $S_{11} = \Delta\varepsilon_1 + \Delta\varepsilon_2$

6 A_2

12. $S_{12} = \Delta r_2 - \Delta r_3 + \Delta r_5 - \Delta r_6$
13. $S_{13} = \theta_2 - \Delta\theta_3 + \Delta\theta_5 - \Delta\theta_6$
14. $S_{14} = \Delta\beta_1 + \Delta\beta_2 - \Delta\beta_3 - \Delta\beta_4$
15. $S_{15} = \Delta\alpha_2 - \Delta\alpha_3 + \Delta\alpha_5 - \Delta\alpha_6$
16. $S_{16} = \Delta\tau_{M1} + \Delta\tau_{M2}$
17. $S_{17} = \Delta\tau_{OH1} + \Delta\tau_{OH2}$

9 B_1

18. $S_{18} = \Delta l_1 - \Delta l_2$
19. $S_{19} = \Delta r_2 + \Delta r_3 - \Delta r_5 - \Delta r_6$
20. $S_{20} = \Delta L_1 - \Delta L_2$
21. $S_{21} = \Delta R_1 - \Delta R_2$
22. $S_{22} = \Delta\eta_1 - \Delta\eta_2$
23. $S_{23} = \Delta\theta_2 + \Delta\theta_3 - \Delta\theta_5 - \Delta\theta_6$
24. $S_{24} = \Delta\alpha_2 + \Delta\alpha_3 - \Delta\alpha_5 - \Delta\alpha_6$
25. $S_{25} = \Delta\beta_1 - \Delta\beta_2 - \Delta\beta_3 + \Delta\beta_4$
26. $S_{26} = \Delta\varepsilon_1 - \Delta\varepsilon_2$

7 B_2

27. $S_{27} = \Delta r_2 - \Delta r_3 + \Delta r_5 - \Delta r_6$
28. $S_{28} = \Delta r_7 - \Delta r_8$
29. $S_{29} = \Delta\theta_2 - \Delta\theta_3 - \Delta\theta_5 + \Delta\theta_6$
30. $S_{30} = \Delta\beta_1 - \Delta\beta_2 + \Delta\beta_3 - \Delta\beta_4$
31. $S_{31} = \Delta\alpha_2 - \Delta\alpha_3 - \Delta\alpha_5 + \Delta\alpha_6$
32. $S_{32} = \Delta\tau_{M1} - \Delta\tau_{M2}$
33. $S_{33} = \Delta\tau_{OH1} - \Delta\tau_{OH2}$

Supplementary table S3. Unscaled normal modes of cis 1,3-propanediol with $\mathbf{C_{2v}}$ symmetry (tTTt) with potential energy distribution (PED) among symmetrized coordinates calculated by BALGA program are compared with the observed bands. Contributions greater than 10% are given. Observed bands typed in italic could not belong to this conformer.v-very, s-strong, m-medium, w-weak, sh-shoulder, br-broad

sym-metry $\mathbf{C_{2v}}$	observed Raman liquid	observed infrared liquid	calculated	PED (%)
A_1				
	3309 vbr	3335 vbr	3835	100 S_1
	2958 sh		3060	99 S_3
	2913	2883	2981	99 S_2
	1476	1474	1535	54 S_9 + 33S_8 + 10S_{10}
	1440	1433	1505	83 S_{10}
	1426	1377	1450	42 S_8 + 39 S_9
	1293	1231	1264	62 S_{11} + 17 S_8
	1097 sh			
	1062	1063	1083	91 S_4
	986	986	1009	54 S_5 + 24 S_{11} + 11 S_7
	412		411	31 S_5 + 28 S_7 + 28 S_6 + 12 S_4
	384			
			197	51 S_6 + 45 S_7
A_2	2958 sh		3004	100 S_{12}
	1316 sh		1312	53 S_{14} + 36 S_{13} + 10 S_{15}
	1238	inactive	1229	78 S_{15} + 23 S_{14}
	871		896	65 S_{13} + 24 S_{14} + 11 S_{15}
	850			
	278		273	99 S_{17}
	---		106	98 S_{16}
B_1				
	3309 vbr	3335 vbr	3835	100 S_{18}
			2972	97 S_{19}
	1476	1474	1525	63 S_{24} + 32 S_{23}
	1440	1422	1461	45 S_{23} + 25 S_{24} + 13 S_{25}
	1318	1355	1328	66 S_{25} + 20 S_{26}
	1193	1184	1200	60 S_{26} + 17 S_{23} + 10 S_{24}
	1039 sh	1038	1054	44 S_{21} + 38 S_{20}
	941	940	1015	61 S_{20} + 36 S_{22}
	920	*921*		
	529	528	461	89 S_{22}
B_2	2958	2945	3109	97 S_{28}
	2887	2883	3011	100 S_{27}
	1293	1292	1308	50 S_{29} + 37 S_{31} + 13 S_{30}
	1196	1184	1171	59 S_{31} + 25 S_{30} + 17 S_{29}
	782	782	784	64 S_{30} + 31 S_{29}
	280		274	99 S_{17}
			114	100 S_{32}

Supplementary table S4. Unscaled normal modes of gGG'g 1,3-propanediol are compared with the observed bands. Potential energy distribution (PED) among symmetrized coordinates is calculated by BALGA program. Contributions greater than 10% are given.v-very, s-strong, m-medium, w-weak, sh-shoulder, br-broad

sym-metry **C_1**	observed Raman liquid	observed Raman cryst 10 K	observed infrared liquid	Calculated gGG'g	PED (%) gGG'g
	3309 w, vbr		3335 vs,vbr		
		3250 m		3829	67 S_{18} + 33 S_1
		3236 mw		3825	67 S_1 + 33 S_{18}
		3135 m, br			
		2978 ms			
	2958 s, sh	2954 s,sh		3099	48 S_{19} + 28 S_{12} + 20 S_{27}
		2943 vs	2945 s	3086	54 S_{12} +35 S_{19}
		2927 s		3063	84 S_{28}
	2913 vs	2908 vs	2883 s	3039	47 S_2 + 45 S_{27}
	2887 vs	2889 m, sh		3017	48 S_3 + 28 S_{27}
		2881 s		3015	43 S_3 + 27 S_2+14 S_{27}
	1476 ms	1477 s	1474 ms	1515	44 S_9 + 37 S_8
		1463 m		1502	55 S_{24} + 27 S_{23}
	1440 m	1450 m		1468	90 S_{10}
			1433 s	1422	42 S_8 + 40 S_9
	1426 m, sh			1400	40 S_{23} + 19 S_{24} + 15 S_{26}
		1413 s		1390	41 S_{25} + 18 S_{13} + 18 S_{15}
		1391 w	1377 ms	1376	26 S_{31} + 22 S_{23} + 20 S_{26}
		1366 w	1355 ms	1364	31 S_{11} + 18 S_{15} + 17 S_{25}
	1316 m,sh	1348 w	1292 m	1281	32 S_{14} + 24 S_{29}
	1294 ms	1294 s	1231 m	1244	30 S_{29} + 22 S_{14} + 15 S_{26}
	1238 m	1228 mw		1160	30 S_{15} + 26 S_{11} + 17 S_{14}
	1193 m	1189 s	1184 m		
	1097 m, sh			1094	28 S_4 + 16 S_{20} + 12 S_{21}
	1062 ms		1063 vs	1075	36 S_{21} + 26 S_{20}
	1040 m, sh		1038 s	1052	23 S_{31} + 19 S_{30} + 17 S_{26}
	986 m		986 s		
	941 m		940 m	949	50 S_{20} + 22 S_{21}
	920 m		921 m	927	25 S_{30} +16 S_7 + 15 S_{29} + 15 S_5
	872 s		869 w	886	64 S_{13} + 17 S_{15}
	850 s		847 w		
	815 w			803	63 S_5 + 16 S_{30} + 15 S_4
	782 w		782 m		
			666 m, vbr	181	60 S_{33} + 36 S_{32}
	529 mw		528 m	515	42 S_7 + 24 S_{30} + 16 S_6
	412 w				
				387	87 S_{17}
	384 w			368	75 S_{22}
				323	32 S_6 + 31 S_{32}
	278 vw				
				125	31 S_{33} + 21 S_6 + 20 S_{32}
				107	82 S_{16} + 10 S_{32}

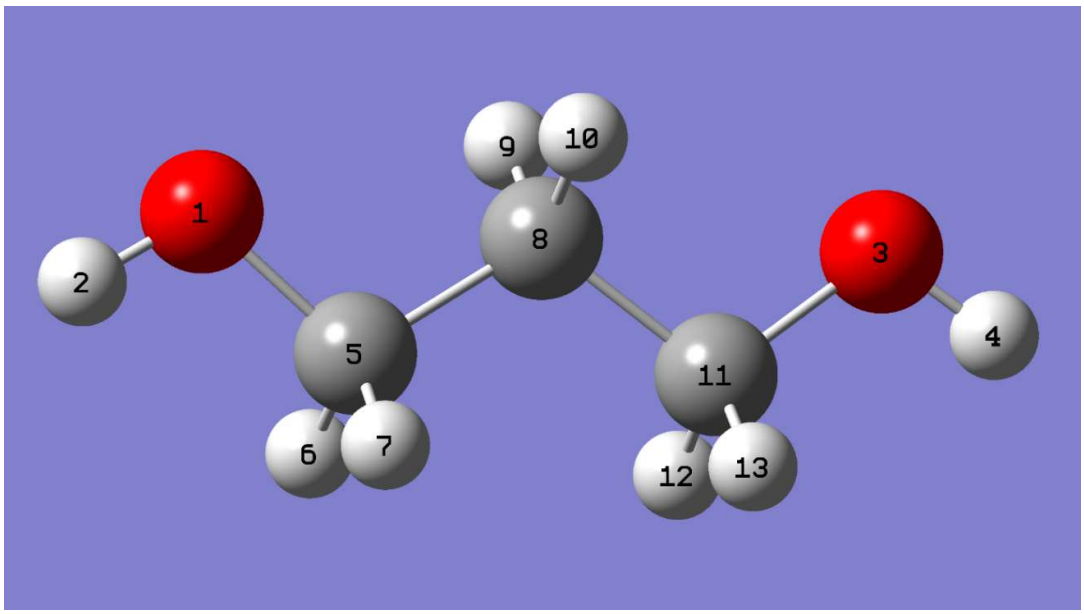

Supplementary figure S1. Labeling of atoms in 1,3-propanediol, tTTt conformer. The list of internal coordinates is given in Supplementary table S1.

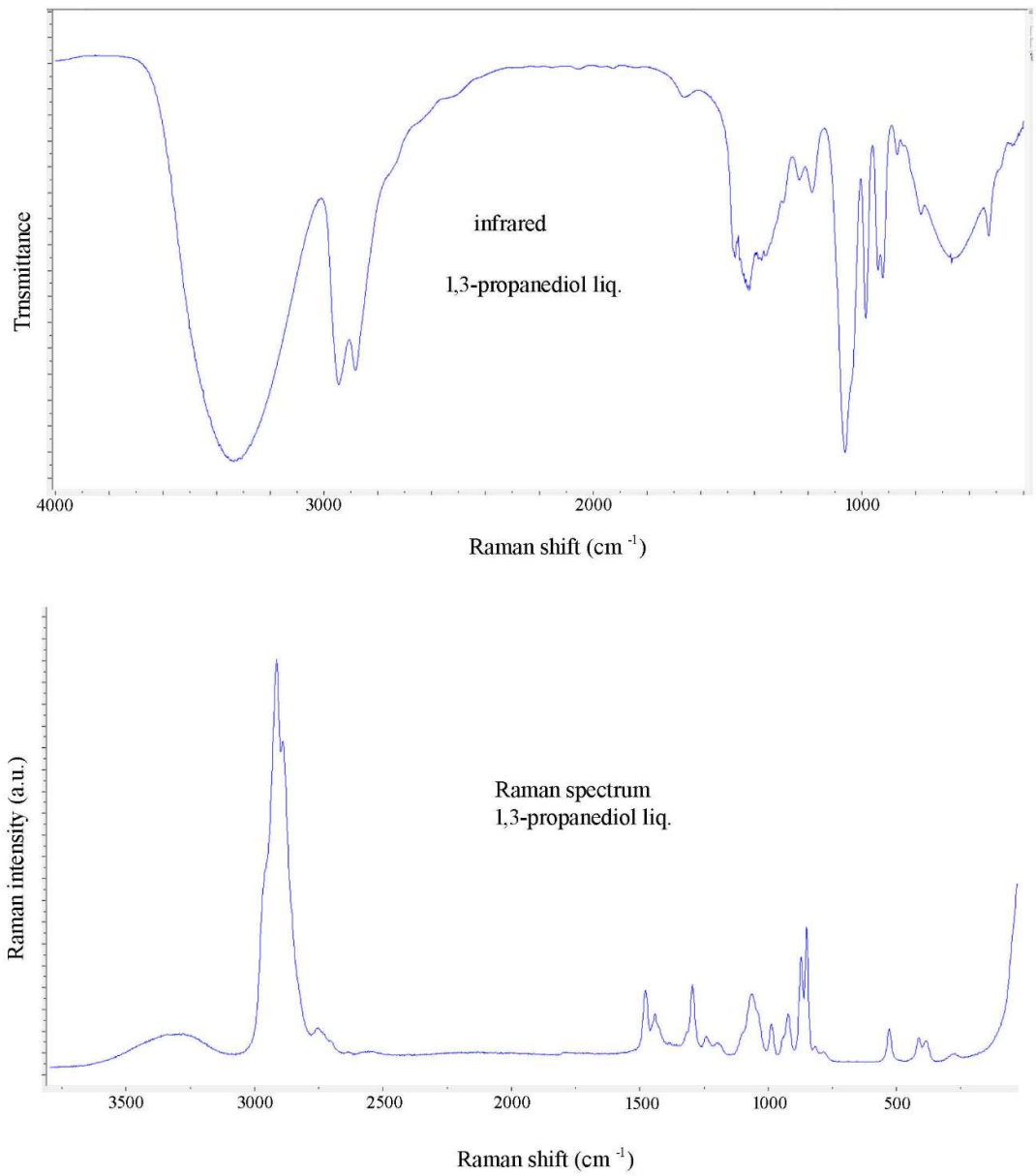

Supplementary figure S2. Comparison of infrared and Raman spectra of liquid 1,3-propanediol.

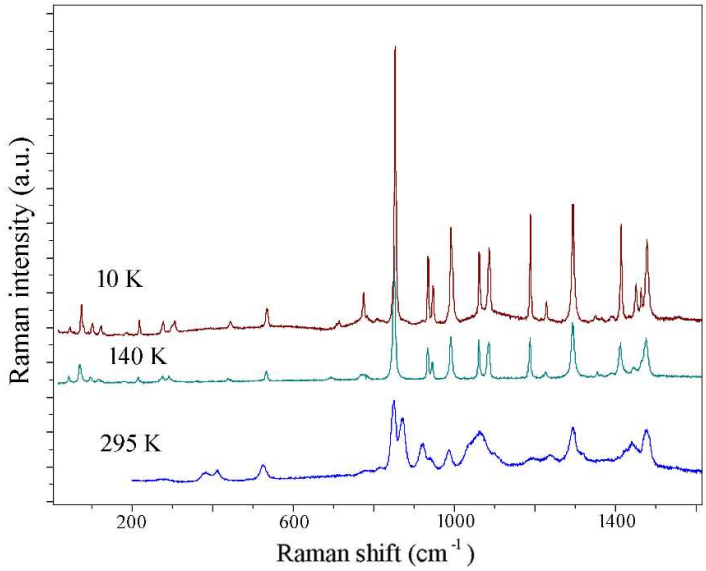

Supplementary figure S3. Low temperature Raman spectra of 1,3-propanediol (10-1600 cm^{-1}).

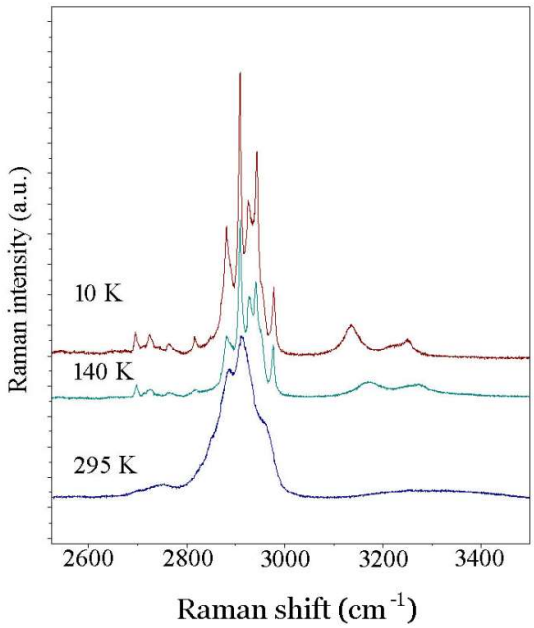

Supplementary figure S4. Low temperature Raman spectra of 1,3-propanediol (2800 -3500 cm $^{-1}$).

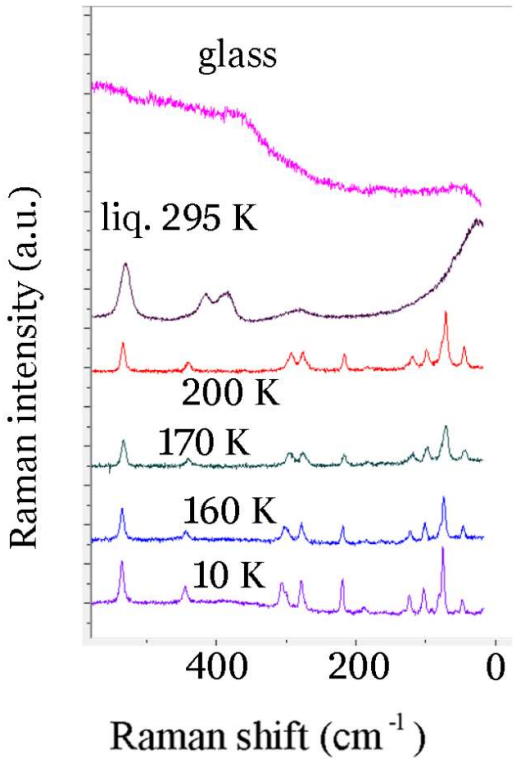

Supplementary figure S5. Comparison of low frequency Raman spectra of liquid (295 K) with Raman spectra of polycrystalline solid 1,3-propanediol (200 K, 170 K, 160 K, 10 K).